Science Bulletin 64 (2019) 516–523

Contents lists available at ScienceDirect

Science Bulletin

journal homepage: www.elsevier.com/locate/scib

Article

High population and dispersion of pentacoordinated Al^V species on the surface of flame-made amorphous silica-alumina

Zichun Wang [a,b], Yijiao Jiang [b], Xianfeng Yi [c], Cuifeng Zhou [a], Aditya Rawal [d], James Hook [d], Zongwen Liu [a], Feng Deng [c], Anmin Zheng [c,*], Michael Hunger [e], Alfons Baiker [f], Jun Huang [a,*]

[a] School of Chemical and Biomolecular Engineering & Sydney Nano Institute, The University of Sydney, New South Wales 2006, Australia
[b] Department of Engineering, Macquarie University, Sydney, New South Wales 2109, Australia
[c] State Key Laboratory Magnetic Resonance & Atomic Molecular Physics, Wuhan Institute of Physics & Mathematics, Chinese Academy of Sciences, Wuhan 430071, China
[d] Mark Wainwright Analytical Centre, University of New South Wales, Sydney, New South Wales 2052, Australia
[e] Institute of Chemical Technology, University of Stuttgart, D-70550 Stuttgart, Germany
[f] Department of Chemistry and Applied Bioscience, ETH Zürich, Hönggerberg, HCI, CH-8093 Zürich, Switzerland

ARTICLE INFO

Article history:
Received 1 January 2019
Received in revised form 2 March 2019
Accepted 26 March 2019
Available online 2 April 2019

Keywords:
Amorphous silica-alumina
Pentacoordinated Al^V species
^{27}Al multiple quantum magic-angle-spinning NMR
H/D exchange

ABSTRACT

Pentacoordinated Al (Al^V) species in silica-alumina are promising to promote the formation of acid sites or act as surface defects for tailoring single-atom catalysts. However, pentahedral coordination (Al^V) is rarely observed in conventionally prepared silica-alumina. Here, we show that high population and dispersion of Al^V species on the surface of amorphous silica-alumina (ASA) can be achieved by means of flame spray pyrolysis. High resolution TEM/EDX, high magnetic-field NMR and DFT calculations are employed to characterize the structure of as-prepared ASAs. Solid-state ^{27}Al multi-quantum MAS NMR experiments show that most of the Al^V species are formed independently from the alumina phase and are accessible for guest molecules on the surface. Upon water adsorption, these Al^V species are transformed to Al^{VI} species, structurally similar to surface Al^{IV} species, as confirmed by DFT calculations. The outstanding catalytic activity of as-synthesized ASA is demonstrated using the in situ H/D exchange reaction with deuterated benzene as an example. The Al^V-rich ASA provides a much lower activation energy (~30 kJ/mol) than that reported for zeolite H-ZSM-5 (~60 kJ/mol). The superior catalytic performance is attributed to the high Al^V content promoting the surface active sites in ASA. The knowledge gained on the synthesis of Al^V-rich ASAs and the nature of aluminum coordination in these materials could pave the way to more efficient silica-alumina based catalysts.

1. Introduction

Alumina and its mixed oxides are important catalytic materials both as active catalysts as well as functional supports for active metal particles. The catalytic functions of these materials in chemical reactions are mainly dependent on the surface coordination of Al species due to their structure-activity relationship. Most research efforts have been focused on the tetrahedral and octahedral coordination (Al^{IV} and Al^{VI}), which are the most popular coordinations of Al species. Pentahedral coordination (Al^V) is rarely observed on alumina and silica-alumina [1–4], and has been proposed to be a transition state to Al^{VI} species generated during calcination of γ-alumina [1,2]. Recently, it has been reported that Al^V species on γ-alumina are surface active sites for stabilizing metal centers or nanoparticles to suppress sintering [5]. The Al^V-metal (e.g., Ba, Cu, Ru, Au, Ag, Pt and Pd) interaction was proposed to improve the catalytic activity of metal centers in various reactions [6–9], such as CO_2 reduction and deNO_x reactions. Therefore, Al^V species have recently attracted great attention, particularly, they were proposed to be coordinatively unsaturated surface centers of supports for anchoring noble metal atoms for emerging single-atom catalysts [5,10].

However, the previous reports showed that Al^V species are not highly populating the surface. Although a certain amount of Al^V species has been found to be generated during phase transformation from γ-Al_2O_3 to α-Al_2O_3 (up to 17%) [1,2], only a very small amount of Al^V species (<2 at.%) was stabilized on the surface of γ-Al_2O_3, when suitable hydroxides or oxides such as La_2O_3 and BaO were added to inhibit the phase transformation and stabilize the unsaturated Al ions. Later, a low content of Al^V species was

* Corresponding authors.
E-mail addresses: zhenganm@wipm.ac.cn (A. Zheng), jun.huang@sydney.edu.au (J. Huang).

https://doi.org/10.1016/j.scib.2019.04.002
2095-9273/

reported to be exclusively distributed on a γ-Al_2O_3 surface [11]. It was also stated that Al^V species only exist nearby Al^{VI} species on the surface of crystalline Al_2O_3 and might represent Al^{VI} in the vicinity of an oxygen vacancy, such as the defect spinel structures of the transition aluminas [12]. In silica-aluminas, Al^V species are considered to be located on the interface between alumina and silica or alumina and aluminosilicates [13]. To our knowledge, silica-alumina with high population of Al^V species accessible for reactants has not been reported up to now. This reinforced the doubt that Al^V species are promising active centers for building high-performance catalysts such as emerging solid acids, single-atom catalysts and spatially confined catalysts due to their poor accessibility [5,10].

Here we show that amorphous silica-aluminas (ASAs) with high population and dispersion of Al^V species on the surface can be prepared by flame spray pyrolysis and that these materials possess interesting catalytic potential. In these materials, Al^V species are well accessible for guest molecules, such as reactants or adsorbates. For example, most of the Al^V species can be converted into Al^{VI} species upon water adsorption, as evidenced by 1D and 2D ^{27}Al MAS NMR studies. These Al^V-rich ASAs exhibit excellent activity in the H/D exchange with benzene-d_6. The local structure of the Al^V species existing on the ASA surface was confirmed by DFT calculations.

2. Experimental

2.1. Preparation of silica-alumina material

ASA catalysts were prepared by flame-spray pyrolysis (FSP) within microseconds, which could combine both synthesis and calcination in a single step at extremely high temperature (ca. 2,000 K). Briefly, the appropriate amount of the precursor materials were dissolved in a 1:1 (vol.%) mixture of acetic acid and methanol. The resulting solution was filtered using a glass filter, pumped through a capillary at a rate of 5 mL min^{-1}, and nebulized at 5 L min^{-1} O_2, and finally ignited by an annular supporting methane/oxygen flame (1.5/0.9 L min^{-1}) to generate ASA nanoparticles. The silica-alumina catalysts are designated as SA/x, where $x = n_{Al}/(n_{Al} + n_{Si}) \times 100$, indicates mol% of the Al precursor in the precursors.

2.2. High-resolution transmission electron microscopy (HRTEM)

HRTEM studies were carried out using a FEI Titan 80/300 ST unit. The instrument was equipped with a Cs corrector for spherical aberration of the objective lens. For imaging, a high-angle annular dark field (HAADF) detector, a GATAN post-column imaging filter was used. In all investigations, the microscope was operated at an acceleration voltage of 300 kV.

2.3. ^{27}Al NMR spectroscopy

Prior to ^{27}Al MQMAS NMR experiments, the samples were dehydrated in glass tubes at 723 K in vacuum at a pressure of less than 10^{-2} bar for 12 h. Subsequently, these samples were transferred into the MAS NMR rotors under dry nitrogen gas inside a glove box. After experiments, the corresponding samples were exposed overnight to the saturated vapor of a $Ca(NO_3)_2$ solution at ambient temperature in a desiccator for full hydration. ^{27}Al MQMAS NMR spectra were recorded on a Bruker Avance III 700 spectrometer with a 16.4 Tesla superconducting magnet operating at a resonance frequency of 182.5 and 700 MHz for ^{27}Al and ^{1}H nuclei, respectively. The samples were packed into 4 mm zirconia MAS rotors fitted with a Kel-F® cap inside a glove box to prevent any exposure to ambient air and moisture. The rotors were spun to 14 kHz MAS in a 4 mm H-X double resonance probe. The MQMAS spectra were acquired using the three-pulse z-filter MQMAS pulse sequence [14]. The 2D spectra were sheared with xfshear program. Excitation and reconversion pulses lasted $\tau_p = 4.2$ and 1.4 μs, respectively, with $\nu_{rf} = 100$ kHz, and the central-transition (CT) selective $\pi/2$ last pulse was 20 μs with $\nu_{rf} = 4.17$ kHz with a repetition time of 0.3 s. The corresponding 1D ^{27}Al MAS NMR spectra were measured on the same spectrometer at a spinning rate of 14 kHz under a single-pulse $\pi/6$ excitation with repetition times of 0.3 s to ensure a complete relaxation of all the signals. The obtained 1D ^{27}Al MAS NMR spectra were decomposed by using Dmfit as a tool [15].

To obtain these parameters, the MQMAS spectrum was evaluated yielding the second-order quadrupolar effect parameter (SOQE) according to:

$$\mathrm{SOQE}^2 = \frac{\delta_{iso} - \delta_{F_2}}{k}, \tag{1}$$

where the isotropic chemical shift δ_{iso} is:

$$\delta_{iso} = \frac{17}{27}\delta_{F_1} + \frac{10}{27}\delta_{F_2}, \tag{2}$$

where δ_{F_1} and δ_{F_2} are the centers of gravity of the signals in the F_1 and F_2 dimension, and

$$k = \frac{3}{10}\frac{4I(I+1) - 3}{[4I(2I-1)\nu_0]^2} \times 10^6, \tag{3}$$

where, spin $I = 5/2$ and Lamor frequency $\nu_0 = 182.5$ MHz for ^{27}Al under study.

The important quadrupole coupling constant C_{QCC} was determined by numerical simulation of the corresponding ^{27}Al MAS NMR spectrum via

$$\mathrm{SOQE} = C_{QCC}\sqrt{1 + (\eta^2/3)}, \tag{4}$$

where η is the asymmetry parameter of the electric field gradient tensor ($0 \le \eta \le 1$).

2.4. DFT calculation studies

DFT calculations were carried out with the Gaussian09 program [16]. ^{27}Al absolute shielding was theoretically calculated using the GIAO (Gauge Including Atomic Orbitals) method [17] at B3LYP/6–311 + G(d,p) level. In order to directly compare the NMR results, the calculated values of ^{27}Al chemical shift were obtained through standard conversion procedure. For the conversion from the calculated absolute isotropic shielding constants (σ) to the relative shifts (δ), the following formula was used for ^{27}Al chemical shift of ASA samples: $\delta(\mathrm{ASA}) = \sigma(\mathrm{ZSM\text{-}5}) + \delta(\mathrm{ZSM\text{-}5}) - \sigma(\mathrm{ASA})$. It is noteworthy that the experimental ^{27}Al chemical shift of Si-Al-O-Si fragment in ZSM-5 was 60 ppm [18], and its absolute isotropic shielding constant was 49.5 ppm predicted at the same theoretical level. Therefore, on the basis of the calculated absolute isotropic shielding constants of each ASA sample, the ^{27}Al chemical shift can be determined theoretically.

2.5. Catalytic test using in situ H/D exchange reaction

Prior to ^{1}H MAS NMR experiments, the samples were filled into 4 mm MAS rotors in a glove box purged with dry nitrogen. Then the samples were dehydrated in glass tubes at 723 K in vacuum at pressure less than 10^{-2} bar for 12 h. The dehydrated samples were loaded in situ with benzene-d_6 (deuteron 99.5%, Cambridge Isotope Laboratories, Inc.) on a vacuum line. ^{1}H MAS NMR studies were carried out on a Bruker Avance III 400 WB spectrometer at a

resonance frequency of 400.1 MHz with a sample spinning rate of ca. 8 kHz. The spectra were recorded after π/2-pulse excitation, with a repetition time of 20 s. The H/D exchange was initiated by heating the MAS rotor in a variable-temperature MAS NMR probe.

3. Results and discussion

The ASA and Al_2O_3 nanoparticles were prepared by flame spray pyrolysis as described previously, offering strong acidity similar to zeolites [19]. All prepared particles had a size around 5–10 nm [20] and their structure has been investigated by X-ray diffraction (XRD), HRTEM, energy dispersive X-ray spectrometry (EDX), and NMR. Powder XRD showed for both ASA samples, containing 10 mol% and 30 mol% of aluminum (SA/10 and SA/30), only a broad reflection at 22° – 23° due to amorphous silica, as shown in the Fig. S1 (online). As a reference, a pure Al_2O_3 sample obtained without adding silica during synthesis has been also shown in Fig. S1 (online). Three broad diffraction peaks at $2\theta = 38.1°$, 46.2° and 67.4°, corresponding to (2 2 2), (4 0 0), and (4 4 0) planes, were observed for crystalline Al_2O_3 due to its small particle size. The very fine nanoparticles with well-ordered lattice structure did not show significant diffraction and could therefore not be identified by XRD.

HRTEM has been applied to examine the existence of alumina phase domains in ASAs [21–23]. For Al_2O_3, the image clearly revealed a well-ordered alumina lattice (Fig. S2a online), in a well agreement with XRD analysis. For ASA samples, the alumina lattice disappeared, and the amorphous nature of both samples was corroborated, as shown in the HRTEM images in Fig. 1a and b. No small alumina clusters were detected on the ASA surface. EDX atom mapping images indicated that Al species were well-distributed in the silica network of SA/10 (Fig. S2b–d online) and SA/30 (Fig. 1c and d). No aggregated aluminum species or small alumina nanoparticles were detectable.

To identify the local coordination of these highly dispersed Al species, solid-state ^{27}Al MAS NMR spectroscopy combined with multiple quantum MAS (MQMAS) has been used to attain the necessary resolution for discriminating among nuclear quadrupole-interaction-broadened signals of the different Al species [14,24,25]. Based on analyzing the ^{27}Al MQMAS spectrum [26–28], the chemical environment parameters, such as δ_{iso}, C_{QCC} and η of Al species can be determined. These parameters enable an accurate quantification of the relative population of the Al species by simulating the corresponding 1D ^{27}Al MAS NMR spectrum [26,29]. In this way, the surface properties of Al species can be probed by the chemical shifts and concentration variation caused by loading the sample with probe molecules, e.g., decreasing the C_{QCC} values of surface Al species upon interaction with H_2O molecules on aluminosilicates [30,31], or partial hydrolysis of surface Al species from the silica network [32–34]. For both, the SA/10 and SA/30 samples, Al^V species have been clearly identified by ^{27}Al MQMAS NMR spectroscopy according to their isotopic chemical shifts along F_1 axis in Fig. 2. The subscript "de" and "hy" are dedicated to species present in dehydrated and hydrated state, respectively. As shown in Fig. 2a and c, two strong signals at (50, 55) and (23, 29) were assigned to Al^{IV} and Al^V species, respectively, indicating their predominant population in the aluminate species on both dehydrated SA/10 and SA/30 samples. Interestingly, only a small peak at (−9, 0.5) and a very weak signal at (−5.4, 2.7) were observed indicating the existence of a very small amount of Al^{VI} species on the dehydrated SA/10 and SA/30 samples, respectively. This observation is distinct from the previous report that Al^V species only exist nearby the alumina phase containing predominantly Al^{VI} species [12].

To quantify the mole fraction of Al^V species in ASA, 1D ^{27}Al MAS NMR spectra of dehydrated SA/10 and SA/30 (shown in Fig. 3a and c) were acquired at a high field of 16.4 T and MAS spinning of 14 kHz. The decomposition and quantitative evaluation of each signal were based on the parameters obtained from ^{27}Al MQMAS NMR spectra (δ_{iso}, C_{QCC}, and η listed in Table 1). The obtained mole fractions of each species has been summarized in Table 2. The mole fraction of Al^V species was 36.9% in SA/10 (with 61.9% Al^{IV} species and 1.2% Al^{VI} species) and 48.7% in SA/30 (with 51.2% Al^{IV} species and 0.1% Al^{VI} species), respectively. The virtual absence of the Al^{VI} species in both samples corroborated the findings of the TEM and EDX measurements that no alumina phase was existing in the silica-alumina materials. As previously reported, Al^V species are generated only in the alumina phase or nearby the alumina phase with dominant Al^{VI} species as encountered in phase transformation of Al_2O_3 [1,2], in the defect spinel structures of the transition aluminas, or at the interface between alumina and silica or silica-alumina [13]. Here, we discovered that a large amount of Al^V species can be produced (mole fraction nearly 50%) on amorphous silica-alumina without concomitant formation of an alumina phase or cluster.

Compared with conventional preparation techniques, FSP provides super-high temperature (up to 2,000 K) and fast cooling rate to produce multi-composition nano-particles in single-step within milliseconds, which is widely used in tailoring materials dominated with metastable phases and polymorphs [35,36], including Al^V species. In the preparation of flame-derived ASA, the Al and Si precursors are well-mixed, then atomized and vaporized to form product vapor, which has been combusted and undergoes nucleation and surface growth to generate ASA nanoparticles. Therefore, the Al atoms can be incorporated throughout the silica matrix, other than self-condensation as often observed in conventional ASAs [37]. The super-high temperature and fast cooling rate may facilitate freezing of metastable Al^V species in the ASA product, and thus, generates Al^V-rich ASA.

As commonly achieved in the synthesis of the aluminosilicate acids, minimizing the formation of the alumina phase or Al^{VI} species during the synthesis can maximize the dispersion of Al atoms and the generation of Al^{IV} species in the silica network or framework for optimal acidity. Therefore, our discovery of the formation

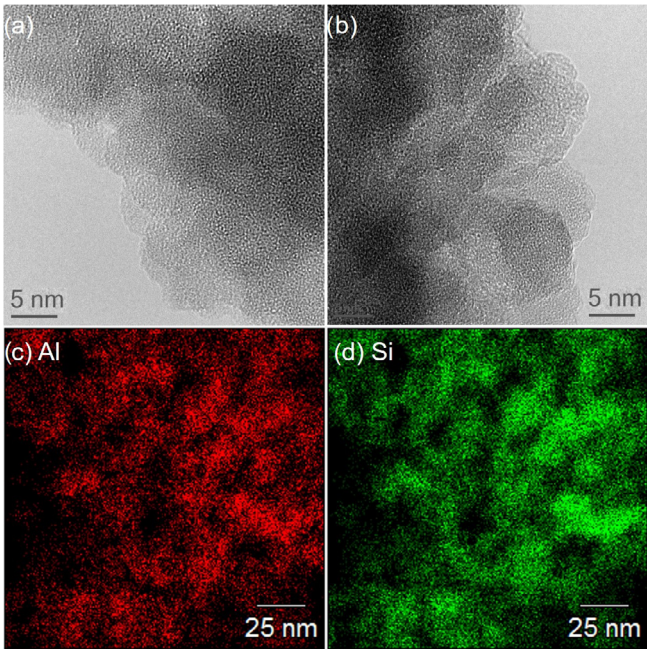

Fig. 1. (Color online) HRTEM images of (a) SA/10 and (b) SA/30 and EDX images of SA/30 (c) Al and (d) Si.

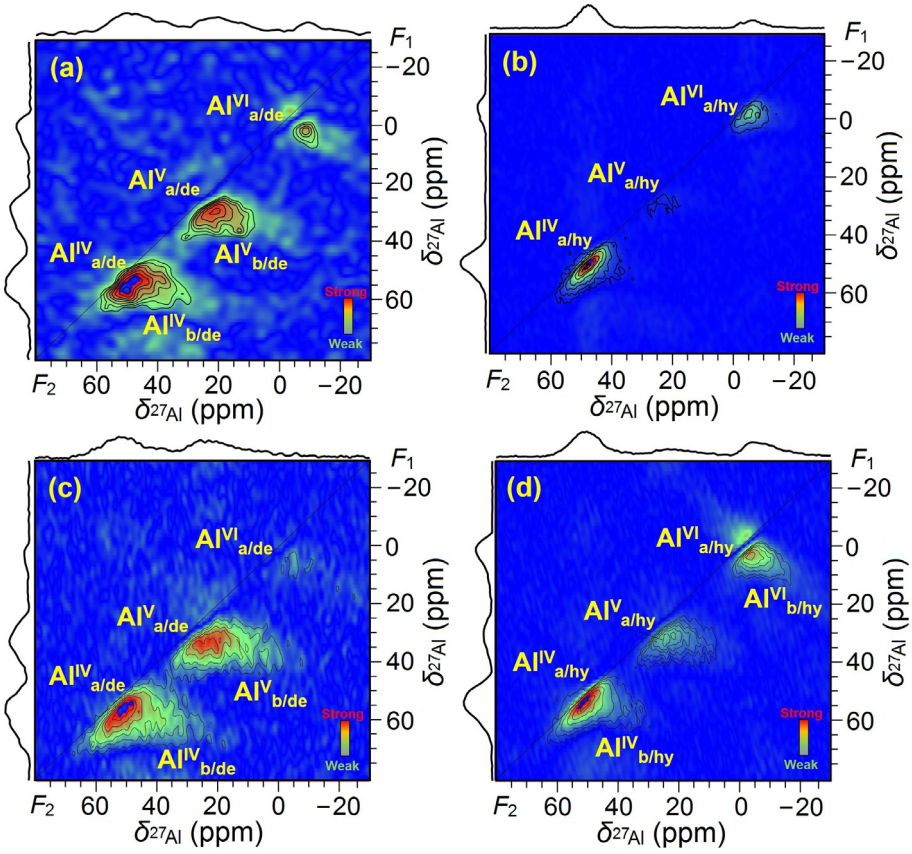

Fig. 2. (Color online) ^{27}Al MQMAS NMR spectra of dehydrated SA/10 (a) and SA/30 (c) state and in corresponding rehydrated state (b) and (d).

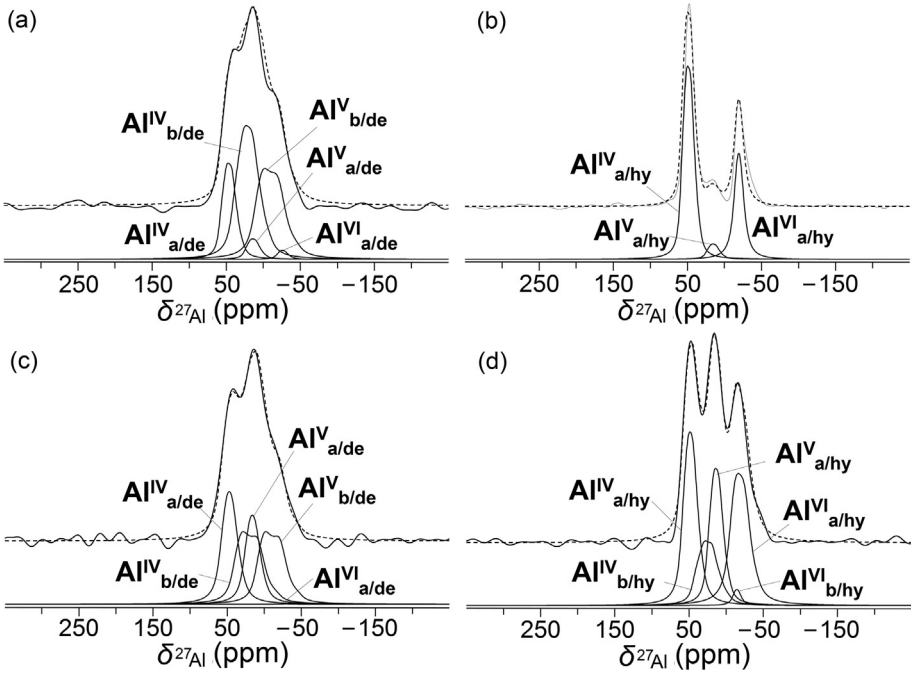

Fig. 3. Deconvolution spectra of ^{27}Al MAS NMR spectra (obtained at 700 MHz magnetic fields) of dehydrated SA/10 (a) and SA/30 (c), and hydrated SA/10 (b) and SA/30 (d), using the parameters listed in Table 1. Experiment (top, solid line), simulation line (top, dash line) and components (bottom, solid lines).

of Al^{V} species independent of the presence of an alumina phase is significant to overcome the current challenge of synthesizing highly dispersed Al^{V} species for high performance catalysts or active materials such as strong acids and emerging single atom catalyst. As an example, recent work revealed Brønsted acid sites can be formed based on Al^{V} species, which can enhance the Brønsted acidity in ASAs [19,38]. Moreover, it has been shown that Al^{V}-rich ASA materials (Al^{V} content >37%) can significantly

Table 1
Summary of parameters and deconvolution results.[a]

	SA10						SA30					
	Dehydrated			Hydrated			Dehydrated			Hydrated		
	δ_{iso} (ppm)	C_{QCC} (MHz)	η	δ_{iso} (ppm)	C_{QCC} (MHz)	η	δ_{iso} (ppm)	C_{QCC} (MHz)	η	δ_{iso} (ppm)	C_{QCC} (MHz)	η
Al_a^{IV}	58	7.7	0.5	58	7.7	0.5	58	7.7	0.5	58	7.7	0.5
Al_b^{IV}	45	11.1	0.3	–	–	–	47	11.1	0.3	47	9.6	0.5
Al_a^{V}	30	7.4	0.5	30	7.4	0.5	31	7.5	0.5	31	7.5	0.5
Al_b^{V}	22	10.9	0.3	–	–	–	20	10.9	0.3	–	–	–
Al_a^{VI}	−5.6	6.3	0.8	1	5.1	0.5	−3	7.6	0.8	1	5.1	0.5
Al_b^{VI}	–	–	–	–	–	–	–	–	–	5	8.6	0.3

[a] Isotropic chemical shifts (δ_{iso}), quadrupole coupling constant (C_{QCC}) and asymmetry parameters of the electric field gradient tensor (η) of each aluminum species, determined by simulation of ^{27}Al MAS NMR spectra of dehydrated and rehydrated SA/10 and SA/30.

Table 2
Concentration of each aluminum species (mol%), determined by simulation of ^{27}Al MAS NMR spectra of dehydrated SA/10 and SA/30, obtained from Fig. 3.

	Al_a^{IV} (%)	Al_b^{IV} (%)	Al_a^{V} (%)	Al_b^{V} (%)	Al_a^{VI} (%)	Al_a^{VI} (%)
SA/10, dehydrated	24.7	37.2	4.4	32.5	1.2	–
SA/10, hydrated	60.7	–	4.2	–	35.1	–
SA/30, dehydrated	28.7	22.5	18.5	30.2	0.1	–
SA/30, hydrated	28.8	16.5	24.9	–	27.8	2

promote the conversion of phenylglyoxal to alkyl mandelates in alcohols, providing up to ~20 times higher turnover frequency than dealuminated zeolite H-Y [20].

Interestingly, both Al^V and Al^{IV} species could co-exist in ASA with high population (mole fraction of nearly 50% for each species). Hitherto it was assumed that Al^{IV} species are available on the surface of ASA or zeolites, but not in high concentration as observed for Al^V species. The surface Al^{IV} species in silica networks or frameworks can interact with adsorbed water molecules to be transformed to Al^{VI} species via partial hydrolysis [34,39], which is useful to investigate whether Al^V species are highly dispersed on the surface and accessible for guest molecules. For that purpose, the dehydrated SA/10 and SA/30 samples were exposed to water molecules and the rehydrated samples were further investigated using ^{27}Al MQMAS NMR spectroscopy. As shown in Fig. 2b and d, the signal for Al^V species was dramatically reduced in 2D NMR spectra and the signals of both Al^{IV} and Al^{VI} species were enhanced. Obviously, most of the Al^V species, formed independently from the alumina phase, were accessible surface species, which were active and interacted with adsorbed water molecules. They were mainly transferred to Al^{VI} species via partial hydrolysis, which was confirmed by the decomposition of corresponding 1D ^{27}Al MAS NMR spectra, as shown in Fig. 3b and d. The high or even complete conversion of Al^V demonstrates that Al^V species are highly accessible to guest molecules and active sites in driving reactions. When introducing a small amount of aluminum (10%) (SA/10), nearly all Al^V species were located on the surface and disappeared after rehydration. This indicates that Al^V species are preferentially located on the surface. With increasing the aluminum content up to 30% (SA/30) part of the Al^V species were formed inside the bulk of the particles and were thus not available for hydrolysis.

Hence, Al^V species are proposed to be highly dispersed in the amorphous silica network via Al^V-O-Si on the surface and their formation is independent of the existence of an alumina phase. To confirm this conclusion and gain further insights into the local structure and geometry of the alumina species, density functional theory (DFT) calculations were applied to find candidate structures for Al^V species in both the dehydrated and the hydrated ASA samples. It is demonstrated that the periodic structure taking into account long-range effects is a quite reliable model to predict the stable states and their reactivity [40–42] for the activated centers of amorphous aluminosilicate surfaces. However, it should be kept in mind that the ASA catalysts in this work were prepared by flame-spray pyrolysis (FSP) technique within microseconds at extremely high temperature (ca. 2,000 K). Cluster models were tentatively used to predict the electronic structures and NMR properties of ASA catalysts in dehydrated and corresponding rehydrated states. Such cluster models composed of silica with Al of the desired coordination number can be used to predict the ^{27}Al chemical shift and C_{QCC} value [43]. The possible structures were optimized at B3LYP/6-31 g(d) theoretical level, and the ^{27}Al chemical shifts and quadrupole parameters (Table S1 online) were predicted at B3LYP/6-311 + G(d,p) theoretical level on the basis of optimized structures. Fig. 4a and c demonstrate that Al^V species could be stabilized and located in the vicinity of SiOH groups on the surface. The corresponding theoretical ^{27}Al chemical shifts are 26 and 21 ppm for Al^V species, similar to the experimental data (20–31 ppm). Upon water adsorption (Fig. 4d and f), most of these Al^V species should be converted to Al^{VI} species at −5 ppm (Table S1 online) with two coordinated water molecules (Fig. 4d), while a fraction of them would be converted into Al^{IV} species at 52 ppm (Fig. 3b and Table S1 (online)). These findings are in line with the NMR experimental results indicating a strong decrease of Al^V signals with enhanced intensities for Al^{VI} and Al^{IV} signals after adsorption of water. Moreover, these mobile water molecules are able to improve the symmetry of Al^V species when coordinated, in good agreement with the lower C_{QCC} values obtained with rehydrated samples. The conversion of the Al^V species in dehydrated states (Fig. 4a and c) to either in Al^{IV} (Fig. 4b) or Al^{VI} (Fig. 4d and f) species rehydrated states, would lead to the decreasing of the C_{QCC} values. The DFT calculations confirm that C_{QCC} values, 12.1, 16.2, and 13.2 MHz (in Al^V species) were changed to 7.7 (in Al^{IV} species), 8.3, and 7.4 MHz (in Al^{VI} species) after hydration, respectively. This behavior is in line with previous theoretical and experimental work on γ-Al_2O_3, silica-alumina, and zeolites, where high C_{QCC} values were always found for Al species on the dehydrated samples and lower ones for highly hydrated surfaces [39]. Besides the aforementioned possibility, the Al^V species could be formed through dehydration reaction between the hydroxyl groups, and thus Al^V species could incorporate into the silica network without being disturbed by SiOH groups, as shown in Fig. 4e. These Al^V species can be transferred into Al^{VI} species upon water loading as well (Fig. 4f). Furthermore, the optimized structures of Al^V species in dehydrated states (Fig. 4a, c and e) with different Al locations have the same stoichiometry ($Al_3H_{15}O_{26}Si_7$), therefore, the relative stabilities can be estimated through the comparisons of the single

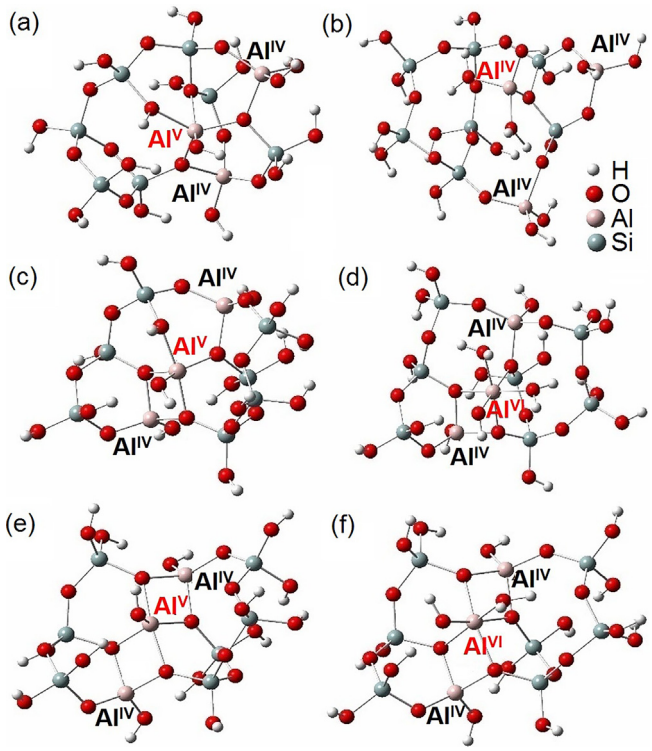

Fig. 4. (Color online) Optimized structure of Al^{V} species in dehydrated states (a, c and e) and in corresponding rehydrated states (b, d and f), both calculated at B3LYP/6-31 g(d) theoretical level. The Al^{V} species in dehydrated states (a, c and e) would be converted to Al^{IV} (b) and Al^{VI} (d and e) species rehydrated states (shown in red), while Al^{IV} species without coordination change before and after rehydrations are shown in black. Parameters determined from DFT calculations were listed in Table S1 (online).

point energy in the theoretical calculation at similar levels. On the basis of the theoretical calculation, the stabilities followed the order: Cluster A < Cluster C < Cluster E. However, the rehydrated states (Fig. 4b, d and f) have different stoichiometries, and their relative stability cannot be compared.

In this research, much more Al^{V} than Al^{IV} species were involved in the hydrolysis on the surface, which indicates that Al^{V} species are more accessible to guest molecules, more prone to generate surface active sites, and more effective in driving reactions. Our recent experiments showed that Al^{V}-rich ASA exhibits excellent catalytic performance for the conversion of phenylglyoxal with various alcohols, better than that of dealuminated zeolite Y, which hitherto was considered to be the most active solid acid in phenylglyoxal conversion [20]. The existence of a large amount of Al^{V} species on the surface is proposed to be the reason for this behavior. Obviously, the presence of Al^{IV} species on ASA is not able to induce higher activity than that of zeolites. On Al_2O_3 and corresponding interfaces, most of Al^{V} species are poorly distributed on the surface and not available for reactants and thus not effective in catalysis.

Silica-alumina catalysts are of great importance in the activation of C—H bonds for hydrocarbon conversion in large scale [44–47]. Here, we tested ASA catalysts having high population and dispersion of Al^{V} species on surface in the hydrogen-deuterium (H/D) exchange with benzene-d_6 to evaluate their catalytic performance in the activation of C—H bonds. Prior to performing H/D exchange between ASA and benzene-d_6, Brønsted acidic zeolite H-ZSM-5 was employed as a reference catalyst, which has been widely used in the H/D exchange studies with benzene-d_6 [44–47]. Three signals at 1.8, 4 and 7.5 ppm (Fig. S3a online) were assigned to terminal SiOH groups, bridging OH (SiOHAl) groups and hydrogen bound to aromatic rings, respectively. After the H/D exchange reaction, the intensity of SiOH groups remained unchanged while the intensity of bridging OH groups decreased with increasing intensity of the aromatic hydrogens. This indicates that the H/D exchange occurred between the benzene-d_6 and acidic OH groups (e.g., SiOHAl), and not the terminal SiOH groups (δ_{1H} = 1.8 ppm) [44,47]. An activation energy of ~60 kJ/mol was obtained in the H/D exchange between H-ZSM-5 benzene d_6, which is similar to that reported in the literature [45].

The stack plot of the ^{1}H MAS NMR spectra recorded at 373 K over SA/30 loaded with benzene d_6 is shown in Fig. S3b (online). The two strong signals at 7.3 and 1.8 ppm were assigned to the aromatic hydrogen atoms and SiOH groups, respectively, while the very weak signal at 0.8 ppm was attributed to few AlOH species. AlOH groups were not active in the H/D exchange reaction, as indicated by their similar intensity before and after reaction. The intensity of SiOH groups simultaneously decreased with increasing intensity of aromatic hydrogen. This observation demonstrates that a H/D exchange reaction occurred between acidic SiOH groups and deuterated benzene since non-acidic SiOH is inactive, as observed with H-ZSM-5. The activation energy of this H/D exchange on ASA was ~30 kJ/mol (Fig. S3c online), which is about half of that obtained for H-ZSM-5 (~60 kJ/mol). Hence, the generation of a large amount of surface Al^{V} species can significantly enhance Brønsted acidity of SiOH groups on ASA [19], which likely promotes the H/D exchange with benzene-d_6 resulting in a lower activation energy compared to that of zeolite H-ZSM-5.

4. Conclusions

The present study indicates that highly dispersed Al^{V} species, being structurally similar to Al^{IV} species, can be formed with high population density on the surface of amorphous silica-alumina. Unlike in the alumina phase or corresponding interfaces, where the Al^{V} species only exist in limited amount and show low surface availability, the new structural environment of Al^{V} species discovered promotes a high surface population of Al^{V} species and these species are highly accessible for guest molecules. The Al^{V}-rich ASA is shown to promote the H/D exchange with benzene-d_6 with an activation energy, which is about half of that obtained with zeolite H-ZSM-5. This finding could pave the way to maximize the efficiency of Al species as unique active centers for new solid acids or single-atom catalyst.

Conflict of interest

The authors declare that they have no conflict of interest.

Acknowledgments

Jun Huang, Zichun Wang, Zongwen Liu, and Cuifeng Zhou acknowledge the financial supports by Australian Research Council Discovery Projects (DP150103842) and Discovery Earlier Career Research Project (DE190101618), the Faculty's MCR Scheme, Energy and Materials Clusters at the University of Sydney. Anmin Zheng and Feng Deng acknowledge the support by the National Natural Science Foundation of China (21522310, 21473244 and 21210005). The Mark Wainwright Analytical Centre at University of New South Wales is acknowledged for access to the solid state NMR spectrometer funded through ARC LIEF LE0989541.

Author contributions

Jun Huang and Yijiao Jiang designed the study. Yijiao Jiang and Alfons Baiker prepared the samples. Zichun Wang, Aditya Rawal, James Hook, and Jun Huang performed the NMR experiments and

structural assignation. Cuifeng Zhou and Zongwen Liu performed the HRTEM microscopy. Xianfeng Yi and Anmin Zheng performed the structure calculations. Jun Huang supervised the scientific work. Jun Huang and Zichun Wang contributed to writing the paper. Alfons Baiker, Feng Deng and Michael Hunger revised the paper.

Appendix A. Supplementary data

Supplementary data to this article can be found online at https://doi.org/10.1016/j.scib.2019.04.002.

References

[1] Duevel A, Romanova E, Sharifi M, et al. Mechanically induced phase transformation of γ-Al_2O_3 into α-Al_2O_3. Access to structurally disordered γ-Al_2O_3 with a controllable amount of pentacoordinated Al sites. J Phys Chem C 2011;115:22770–80.
[2] Sepelak V, Duevel A, Wilkening M, et al. Mechanochemical reactions and syntheses of oxides. Chem Soc Rev 2013;42:7507–20.
[3] Lippmaa E, Samoson A, Magi M. High-resolution aluminum-27 NMR of aluminosilicates. J Am Chem Soc 1986;108:1730–5.
[4] Chen FR, Davis JG, Fripiat JJ. Aluminum coordination and Lewis acidity in transition aluminas. J Catal 1992;133:263–78.
[5] Kwak JH, Hu J, Mei D, et al. Coordinatively unsaturated Al^{3+} centers as binding sites for active catalyst phases of platinum on γ-Al_2O_3. Science 2009;325:1670–3.
[6] Kwak JH, Kovarik L, Szanyi J. CO_2 reduction on supported Ru/Al_2O_3 catalysts: cluster size dependence of product selectivity. ACS Catal 2013;3:2449–55.
[7] Thomas JM, Saghi Z, Gai PL. Can a single atom serve as the active site in some heterogeneous catalysts? Top Catal 2011;54:588–94.
[8] Deng H, Yu Y, Liu F, et al. Nature of Ag species on Ag/γ-Al_2O_3: a combined experimental and theoretical study. ACS Catal 2014;4:2776–84.
[9] Shi L, Deng GM, Li, et al. Al_2O_3 nanosheets rich in pentacoordinate Al^{3+} ions stabilize Pt-Sn clusters for propane dehydrogenation. Angew Chem Int Ed 2015;54:13994–8.
[10] Yang M, Li S, Wang Y, et al. Catalytically active Au-O$(OH)_x$-species stabilized by alkali ions on zeolites and mesoporous oxides. Science 2014;346:1498–501.
[11] Lee D, Duong NT, Lafon O, et al. Primostrato solid-state NMR enhanced by dynamic nuclear polarization: pentacoordinated Al^{3+} ions are only located at the surface of hydrated γ-alumina. J Phys Chem C 2014;118:25065–76.
[12] MacKenzie KJD, Temuujin J, Okada K. Thermal decomposition of mechanically activated gibbsite. Thermochim Acta 1999;327:103–8.
[13] Dewitte BM, Grobet PJ, Uytterhoeven JB. Pentacoordinated aluminum in noncalcined amorphous aluminosilicates, prepared in alkaline and acid-medium. J Phys Chem 1995;99:6961–5.
[14] Amoureux JP, Fernandez C, Steuernagel S. ZFiltering in MQMAS NMR. J Magn Reson Ser A 1996;123:116–8.
[15] Massiot D, Fayon F, Capron M, et al. Modelling one- and two-dimensional solid-state NMR spectra. Magn Reson Chem 2002;40:70–6.
[16] Frisch MJT, Schlegel HB, Scuseria GE, et al. Gaussian 09, revision B.01. Wallingford, CT: Gaussian Inc; 2010.
[17] Cheeseman JR, Trucks GW, Keith TA, et al. A comparison of models for calculating nuclear magnetic resonance shielding tensors. J Chem Phys 1996;104:5497–509.
[18] Yu Z, Li S, Wang Q, et al. Brønsted/Lewis acid synergy in H-ZSM-5 and H-MOR zeolites studied by ^1H and ^{27}Al DQ-MAS solid-state NMR spectroscopy. J Phys Chem C 2011;115:22320–7.
[19] Huang J, van Vegten N, Jiang Y, et al. Increasing the Brønsted acidity of flame-derived silica/alumina up to zeolitic strength. Angew Chem Int Ed 2010;49:7776–81.
[20] Wang Z, Jiang Y, Baiker A, et al. Efficient acid-catalyzed conversion of phenylglyoxal to mandelates on flame-derived silica/alumina. ACS Catal 2013;3:1573–7.
[21] Reller A, Cocke DL. High resolution transmission electron microscopic (HRTEM) determination of the preferentially exposed faces on γ-Al_2O_3 and η-Al_2O_3. Catal Lett 1989;2:91–5.
[22] Wang Z, Pokhrel S, Chen M, et al. Palladium-doped silica-alumina catalysts obtained from double-flame FSP for chemoselective hydrogenation of the model aromatic ketone acetophenone. J Catal 2013;302:10–9.
[23] Nassreddine S, Massin L, Aouine M, et al. Thiotolerant Ir/SiO_2-Al_2O_3 bifunctional catalysts: effect of metal-acid site balance on tetralin hydroconversion. J Catal 2011;278:253–65.
[24] Yu Z, Zheng A, Wang Q, et al. Insights into the dealumination of Zeolite HY revealed by sensitivity-enhanced ^{27}Al DQ-MAS NMR spectroscopy at high field. Angew Chem Int Ed 2010;49:8657–61.
[25] Frydman L, Harwood JS. Isotropic spectra of half-integer quadrupolar spins from bidimensional magic-angle-spinning NMR. J Am Chem Soc 1995;117:5367–8.
[26] Jiao J, Kanellopoulos J, Wang W, et al. Characterization of framework and extra-framework aluminum species in non-hydrated zeolites Y by ^{27}Al spin-echo, high-speed MAS, and MQMAS NMR spectroscopy at B_0=9.4 to 17.6 T. Phys Chem Chem Phys 2005;7:3221–6.
[27] Alemany LB, Steuernagel S, Amoureux JP, et al. Very fast MAS and MQMAS NMR studies of the spectroscopically challenging minerals kyanite and andalusite on 400, 500, and 800 MHz spectrometers. Solid State Nucl Magn Reson 1999;14:1–18.
[28] Goldbourt A, Landau MV, Vega S. Characterization of aluminum species in alumina multilayer grafted MCM-41 using ^{27}Al FAM(II)-MQMAS NMR. J Phys Chem B 2003;107:724–31.
[29] Gore KU, Abraham A, Hegde SG, et al. ^{29}Si and ^{27}Al MAS/3Q-MAS NMR studies of high silica USY zeolites. J Phys Chem B 2002;106:6115–20.
[30] Jiao J, Kanellopoulos J, Behera B, et al. Effects of adsorbate molecules on the quadrupolar interaction of framework aluminum atoms in dehydrated zeolite H Na-Y.. J Phys Chem B 2006;110:13812–8.
[31] Li SH, Zheng AM, Su YC, et al. Extra-framework aluminium species in hydrated faujasite zeolite as investigated by two-dimensional solid-state NMR spectroscopy and theoretical calculations. Phys Chem Chem Phys 2010;12:3895–903.
[32] Guth JL, Kessler H. Catalysis and zeolites-fundamentals and applications. New York: Springer-Verlag; 1999.
[33] O'Malley K, Gil A, Curtin T. Synthesis of mesoporous aluminophosphates-based materials using various copolymers as templates. Microporous Mesoporous Mater 2014;191:48–58.
[34] Wouters BH, Chen TH, Grobet PJ. Reversible tetrahedral-octahedral framework aluminum transformation in zeolite Y. J Am Chem Soc 1998;120:11419–25.
[35] Strobel R, Pratsinis SE. Flame aerosol synthesis of smart nanostructured materials. J Mater Chem 2007;17:4743–56.
[36] Koirala R, Pratsinis SE, Baiker A. Synthesis of catalytic materials in flames: opportunities and challenges. Chem Soc Rev 2016;45:3053–68.
[37] Matsumoto A, Chen H, Tsutsumi K, et al. Novel route in the synthesis of MCM-41 containing framework aluminum and its characterization. Microporous Mesoporous Mater 1999;32:55–62.
[38] Wang Z, Jiang Y, Lafon O, et al. Brønsted acid sites based on penta-coordinated aluminum species. Nat Commun 2016;7:13820.
[39] Bourgeatlami E, Massiani P, Direnzo F, et al. Study of the state of aluminum in zeolite-beta. Appl Catal 1991;72:139–52.
[40] Handzlik J, Grybos R, Tielens F. Isolated chromium(VI) oxide species supported on Al-modified silica: a molecular description. J Phys Chem C 2016;120:17594–603.
[41] Yun D, Yun YS, Kim TY, et al. Mechanistic study of glycerol dehydration on Brønsted acidic amorphous aluminosilicate. J Catal 2016;341:33–43.
[42] Chizallet C, Raybaud P. Pseudo-bridging silanols as versatile Brønsted acid sites of amorphous aluminosilicate surfaces. Angew Chem Int Ed 2009;48:2891–3.
[43] Lam E, Comas-Vives A, Copéret C. Role of coordination number, geometry, and local disorder on ^{27}Al NMR chemical shifts and quadrupolar coupling constants: case study with aluminosilicates. J Phys Chem C 2017;121:19946–57.
[44] Huang J, Jiang Y, Marthala VRR, et al. In situ ^1H MAS NMR investigations of the H/D exchange of alkylaromatic hydrocarbons on zeolites H-Y, La, Na-Y, and H-ZSM-5. Microporous Mesoporous Mater 2007;99:86–90.
[45] Haw JF. Zeolite acid strength and reaction mechanisms in catalysist. Phys Chem Chem Phys 2002;4:5431–41.
[46] Beck LW, Xu T, Nicholas JB, et al. Kinetic NMR and density-functional study of benzene H/D exchange in zeolites, the most simple aromatic-substitution. J Am Chem Soc 1995;117:11594–5.
[47] White JL, Beck LW, Haw JF. Characterization of hydrogen-bonding in zeolites by proton solid-state NMR-spectroscopy. J Am Chem Soc 1992; 114:6182–9.

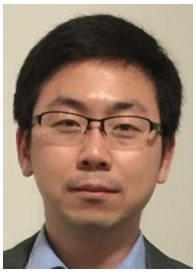

Zichun Wang received Ph.D. degree from the University of Sydney in 2015. After three years postdoctoral researches at the University of Sydney and Case Western Reserve University, he joined Macquarie University, Sydney, and currently an Australia Research Center Discovery Early Career Research Award fellow. His research interests focus on rational design of heterogeneous catalysts through in situ spectroscopic studies on catalyst structure and reaction mechanism, applied for green and sustainable energy and chemical production.

Anmin Zheng obtained his Ph.D. degree (2005) from Wuhan Institute of Physics and Mathematics (WIPM), Chinese Academy of Sciences and then has been affiliated with WIPM afterwards. He was promoted to Professor in 2012. His research interest has been focusing on structure and reaction mechanism of the solid acid catalysts by using experimental solid-state NMR and theoretical quantum chemical calculations.

Jun Huang is an Associate Professor at the University of Sydney. He received his Ph.D. degree from University of Stuttgart in 2008 and joined Sydney in 2010 after his postdoctoral fellow at Georgia Institute of Technology and ETH Zürich. His research is to develop emerging catalytic technologies for more attractive, practical, and cleaner processes using in situ spectroscopic techniques, coupled with new catalyst design and innovative reaction engineering.